Experimental Eye Research 195 (2020) 108031

Contents lists available at ScienceDirect

Experimental Eye Research

journal homepage: www.elsevier.com/locate/yexer

Primate model of chronic retinal neovascularization and vascular leakage

Chintan Patel[a,*], Robin Goody[a], Wenzheng Hu[a], Anish Kurian[a], Donnicia James[a], Richard Torres[b], Lori-Ann Christie[c], Thomas Hohman[d], Matthew Lawrence[a]

[a] Virscio, Inc., 4 Science Park, New Haven, CT 06511, USA
[b] Department of Laboratory Medicine, Yale School of Medicine, New Haven, CT 06510, USA
[c] Department of Biological Sciences, Allergan plc, 2525 Dupont Drive, Irvine, CA 92612, USA
[d] Envision Consulting, LLC, 2009 Glenwood Dr, Ocean City, NJ 08226, USA

A B S T R A C T

The purpose of this study was to characterize and develop a primate model of chronic retinal neovascularization and vascular leakage that can be employed to assess efficacy of experimental therapeutics targeting retinal ischemic and neovascular diseases. African green monkeys received bilateral intravitreal (IVT) injection of DL-alpha-aminoadipic acid (DLAAA; 5 mg) following ophthalmic examination, color fundus photography, fluorescein angiography (FA) and optical coherence tomography (OCT). Imaging was repeated to evaluate progression and subsequent stabilization of retinal vascular pathology elicited by DLAAA. Aflibercept (Eylea) was administered IVT (1.4 mg) to assess effects on vascular leakage. Ocular tissue was collected for histopathology and glial fibrillary acidic protein (GFAP), von Willebrand Factor (vWF), CD105/endoglin, VEGF and CD68 immunohistochemistry to study retinal degeneration and vascular remodeling. IVT DLAAA administration resulted in telangiectatic vessel formation as early as two-weeks post-injection, followed by retinal vascular leakage and inner retinal edema. Neovascular lesion progression was evident up to 8–10 weeks post-injection before stabilizing into a vascular leakage state that persisted beyond 90 weeks. Histopathology and immunostaining revealed retinal degeneration and neovascularization, increased expression of vWF, CD105/endoglin, VEGF and CD68 immunoreactivities in addition to Müller cell loss. Aflibercept significantly attenuated vascular leakage for 2–4 weeks before progressive return of leakage from weeks 4–8. Lesions remained responsive to anti-VEGF administration at 90 weeks after DLAAA injection. Findings support application of the primate DLAAA-induced retinal vascular leakage model for efficacy evaluations of candidate therapeutics and sustained release strategies targeting exudative AMD, diabetic retinopathy, macular telangiectasia and other retinal ischemic and neovascular diseases. Findings confirm relevance of the DLAAA primate phenotype to understanding shared retinal vascular disease mechanisms and macular susceptibility to vascular and metabolic insults.

1. Introduction

Retinal vascular diseases such as exudative age-related macular degeneration (eAMD), diabetic macular edema (DME) and proliferative diabetic retinopathy (PDR) exhibit retinal microvasculature pathology contributing to enduring and progressive vascular leakage and aberrant neovascularization. Choroidal neovascularization (CNV) is a key feature of eAMD where pathological neovessels grow from choroidal blood vessels and breach Bruch's membrane to penetrate and disrupt the subretinal space. CNV vessels are immature with a more permeable endothelium, devoid of endothelial cell tight junctions and pericyte integration, leading to fluid accumulation and hemorrhage that can result in blindness. In DME and PDR, damage induced by hyperglycemia leads to ischemia and inflammation, which contribute to persistent fluid accumulation and retinal neovascularization (RNV) into the vitreous and inner retina, resulting in retinal detachment and blindness (Antonetti et al., 2012; Grossniklaus et al., 2010).

In these prevalent neovascular and ischemic diseases, vascular endothelial growth factor (VEGF) is a key mediator of endothelial destabilization leading to persistent vascular permeability and choroidal or retinal neovascularization. Bevacizumab, ranibizumab and aflibercept, current standard of care interventions for CNV, DME and PDR, bind and neutralize VEGF to limit its pathological effect, and are routinely prescribed with significant, but often selective and transient efficacy. Although most patients benefit from anti-VEGF therapy, the limited duration of action of these therapeutics necessitates intravitreal (IVT) injections as frequently as every month for optimal effect. Less frequent, less optimal dosing regimens are more often pursued as a compromise to mitigate the significant patient, physician and cost burden of monthly IVT injections, and associated risks. As such, there is a significant need on the part of patients and health care providers for novel and/or anti-VEGF therapies of longer duration of action that can effectively stabilize the vasculature and regress pathological neovascularization across broad patient populations.

A challenge with historically available models of retinal vascular diseases in species that closely emulate the human eye, such as non-human primates (NHPs), is the absence of chronic vascular leakage and/or a neovascular response characteristic of human eAMD, DME and

* Corresponding author.
E-mail address: cpatel@virscio.com (C. Patel).

https://doi.org/10.1016/j.exer.2020.108031
Received 1 November 2019; Received in revised form 31 March 2020; Accepted 1 April 2020
Available online 07 April 2020

PDR. In the rodent and NHP laser-induced CNV models of eAMD, transient vascular leakage and neovascular response from the choroidal vasculature progresses for 2–3 weeks post-laser disruption of Bruch's membrane and spontaneously regresses thereafter. While regression of this induced pathology is accelerated by anti-VEGF treatments, in humans CNV pathology returns and persists following washout of anti-VEGF agents. Therefore, a model of persistent and recurring vascular leakage and neovascularization would significantly aid and accelerate evaluation of longer-acting interventions to address the multiple clinical manifestations of pathological vascular instability and neovascularization.

One such model of chronic leakage that has been described in the rat (Shen et al., 2010) and rabbit (Cao et al., 2018; Li et al., 2018), and is already routinely employed for candidate screening purposes in these species, is the DL-alpha-aminoadipic (DLAAA) model. DLAAA is a selective glial cytotoxin reported to cause glial dysfunction and death by suppressing action of glutamine synthetase (Kato et al., 1990, 1993; Linser and Moscona, 1981), and compromising broader Müller cell retinal homeostatic functions leading to breakdown of the blood-retinal barrier (Shen et al., 2010). Subretinal injection of DLAAA disrupted blood-retinal barrier and increased leakage and tortuosity of vessels up to two months post-injection in adult rats (Shen et al., 2010). Several groups have recently demonstrated increased vascular leakage and RNV up to 12–18 months following IVT administration of DLAAA in rabbits and inhibition of such pathology by anti-VEGF agents aflibercept, ranibizumab, bevacizumab (Cao et al., 2018; Li et al., 2018) and DARPins targeting VEGF-A_{165} (Rodrigues et al., 2018). Retinal vasculature and neuronal anatomy differ in rats, rabbits and humans, but are substantially shared between monkeys and humans. Retinal vasculature, retinal segmentation and basal lamina boundaries, proportionate abundance of retinal neuronal and glial cell subtypes, and the presence of a macula are homologous in monkeys and humans (Mustari, 2017). Here we report a novel NHP model of chronic vascular leakage induced by DLAAA that recapitulates pathology demonstrated in the rat and rabbit models, but develops uniquely within the anatomy of the primate retina to emulate clinical RNV, sharing elements of eAMD, DME and PDR and most strikingly, macular telangiectasia (MacTel) (Yannuzzi et al., 2006). This preclinical model of chronic retinal vascular leakage and neovascularization allows efficacy screening of both short and long-acting anti-angiogenic compounds at multiple stages of disease development.

2. Methods

2.1. Animals

A total of eight adult male and nine female African green monkeys (*Chlorocebus. Sabaeus*) (males: 5.2–6.9 kg; females: 3.1–4.1 kg) were used in accordance with the ARVO Statement for the Use of Animals in Ophthalmic and Vision Research. Approvals allowing bilateral treatments and conduct of the animal studies were obtained from the primate facility at St. Kitts Biomedical Research Foundation in St. Kitts, West Indies. Prescreen ophthalmic examination, comprising slit lamp (SL) examination, color fundus photography (CFP), fluorescein angiography (FA) and optical coherence tomography (OCT) were conducted to confirm absence of pre-existing ocular abnormalities. Monkeys were observed twice daily in their home cages for behavioral changes and overall wellbeing. Additional monitoring was conducted during scheduled ophthalmic examinations. Animals were pair-housed following completion of animal enrollment and treatment group assignments six to nine weeks after DLAAA administration. Monkey weights were measured at study recruitment and at defined time points. Monkeys were anesthetized with ketamine/xylazine [8.0 mg/kg ketamine (Fort Dodge)/1.6 mg/kg xylazine (Lloyd Lab)] in a sterile, mixed cocktail for all procedures.

2.2. DLAAA model induction

On day 0 all enrolled monkeys received IVT injections of DLAAA (5 mg, Sigma-Aldrich product code A0637, St. Louis, MO) in both eyes (OU). DLAAA was dissolved in 1M hydrochloric acid to generate a 100 mg/mL stock solution, which was then diluted with phosphate buffered saline (PBS; Sigma-Aldrich St. Louis, MO), pH adjusted to 7.4 and filtered through a 0.2-micron filter. Aliquots of DLAAA dose solutions (25 mg/mL) were prepared before the day of dosing and stored at −80 °C. At the time of IVT dosing the required amount of frozen DLAAA solution aliquots were removed from the freezer and thawed to room temperature prior to loading into dosing syringes. All aliquots were prepared from a single batch of DLAAA. Prior to IVT dosing, topical 1% atropine was applied to each eye to achieve full pupil dilation. The ocular surface was anesthetized with 1–2 drops of 0.5% proparacaine (Sandoz, Switzerland) and prepared aseptically with 5% Betadine (Alcon, Fort Worth, TX) followed by sterile 0.9% saline (Hospira, Lake Forest, IL). A vitreous tap was performed with a 1 mL syringe attached to a 27-gauge needle to remove 100 μL of vitreous humor, which was then stored at −80°C. Vitreous taps were performed prior to DLAAA dosing to limit intraocular pressure elevation. Vitreous taps were successfully performed in 70% of the eyes with vitreous viscosity preventing this procedure in the remaining eyes, although all eyes were subsequently dosed with DLAAA. DLAAA solution (5 mg/200 μL) was delivered to the mid-vitreous 3 mm posterior to the limbus in the inferior temporal quadrant using 0.3 cc insulin syringes with a 31G 0.5-inch needle. Injections were immediately followed by topical administration of triple antibiotic ointment (neomycin/polymyxin B sulfates/bacitracin zinc; Bausch + Lomb, Rochester, NY) and 1% atropine ointment (Bausch + Lomb, Rochester, NY). In instances where DLAAA-induced pathology was severe or retinal detachment was observed, the eye was excluded from further analysis. The pre-defined criteria for exclusion included 1) the development of severe pathology with large or widespread leakage that reached beyond the vascular arcades or extended into the peripheral retina, 2) eyes with severe hemorrhage, or 3) retinal detachment, resulting from a combination of edema and tractional forces from fibrosis and tissue remodeling resulting in serous or complete retinal detachment. Applying these criteria resulted in exclusion of 25% of animals receiving DLAAA.

2.3. Anti-VEGF delivery

Following ophthalmic examinations at weeks 8 or 9 following DLAAA treatment, fluorescein angiography images were graded by a masked assessor to evaluate severity of DLAAA-induced retinal neovascular leakage, referencing a standard leakage scoring scale (see Table 1). Animals were stratified based on cumulative scores in both eyes and assigned to treatment groups to achieve balanced severity of baseline DLAAA-induced pathology. FA imaging was repeated at week 10 prior to treatments to confirm animal assignments and capture baseline FA images. Prior to anti-VEGF IVT dosing the ocular surface was anesthetized with 1–2 drops of 0.5% proparacaine and prepared aseptically with 5% Betadine followed by sterile 0.9% saline. Anti-VEGF treatments were delivered IVT to monkeys using sterile 0.3 mL insulin syringes pre-fitted with 31G 5/16” needles (Ulticare, Excelsior, MN). The needle was placed 2 mm posterior to the limbus in the inferior temporal quadrant, targeting the central vitreous. Eyes received a single IVT injection of either vehicle (0.9% saline, 50 μL) or aflibercept (35 μL of 40 mg/mL solution; Eylea®, Regeneron, Tarrytown, NY). Dose levels of anti-VEGF agents were selected based on relative vitreous volume of African Green monkeys (approximately 2.7 mL) and comparative human vitreous volume of 4.4 mL (Weir and Collins, 2013). All contralateral eyes received identical treatment. Injections were followed by topical administration of neomycin/polymyxin B sulfates/bacitracin antibiotic ointment. Dosing was conducted over 2 days and follow-up examination schedules were maintained for the duration of the study.

Table 1
Graded leakage scoring scale.

Lesion size score		Leakage severity score	
0	Absent	0	Absent
1	Leakage confined to macula	1	Leaky vessels distinguishable at all FA time points
2	Leakage extends beyond macula or a small area of leakage is also apparent in the periphery	2	Leaky vessels distinguishable until later FA time points
3	Leakage extends to vascular arcades or significant leakage in periphery	3	Leak evident at early FA time points spreads up to one disc diameter from affected vessel or in isolated areas of periphery
4	Leakage extends to vascular arcades or more temporal and also present in inferior or temporal periphery	4	Leak evident at early FA time points and spreads beyond a disc diameter from affected vessel(s) or widespread in periphery
5	Leakage spanning both inferior and superior vascular arcades and macula as well as peripheral distribution	5	Leakage evident early and spreads widely across macular region and periphery

2.4. Ophthalmic exams

Eyes were examined by slit lamp biomicroscopy at baseline, biweekly after DLAAA administration and weekly after intervention until study terminus to confirm integrity of the ocular surface, general ocular health, broad ocular response to DLAAA administration and normal response to mydriatics (10% phenylephrine HCl (Akorn, Forest Hill, IL) and 1% cyclopentolate HCl (Sandoz, Holzkirchen, Germany). Ophthalmic findings were graded using a modified version of the Hackett-McDonald scoring system (Liu et al., 2017)

2.5. Color fundus photography

Bilateral color fundus images of the retina were obtained at baseline, biweekly after DLAAA administration and weekly after intervention until study terminus with 50° field of view centered on the fovea using a Topcon TRC-50EX retinal camera with Canon 6D digital imaging hardware and New Vision Fundus Image Analysis System software.

2.6. Fluorescence angiography

Fluorescence angiograms (FA) were acquired using either a Topcon TRC-50EX retinal camera or a Heidelberg HRA + OCT with high resolution acquisition at fixed gain and flash intensity following intravenous injection of 0.1 mL/kg of 10% sodium fluorescein (Sigma-Aldrich St. Louis, MO). Images were collected up to 6 minutes after fluorescein administration. The retinal area exhibiting vascular leakage in the full series of angiograms was assessed and scored using a graded scoring system, and the total fluorescence intensity within the leaking area in the 1-minute raw angiograms was quantified using a semi-automated multi ROI tool in ImageJ (week 10 to study terminus).

2.7. Leakage analysis

DLAAA-induced leakage was evaluated using a custom grading scale and a multi-ROI automated analysis, and the analysis was limited to select time points showing maximum treatment effect and recurrence of leakage. Relative leakage size and severity were assessed using an independent 5-point “lesion size” and “lesion severity” scales applied in the review of the full FA image series (approximately 5 seconds to 6 minutes after fluorescein administration) by masked observers, and determined values summed to generate an overall 10-point graded leakage scale (Table 1). Both lesion size and lesion severity scales were generated similar to prior scales for other species (Rodrigues et al., 2018) with reference to an image set representative of the range of observed fluorescein signal and distribution exhibited in DLAAA treated eyes with and without anti-VEGF intervention. Absolute fluorescence intensity was measured using FA images acquired 1 minute after fluorescein injection. Custom grids were developed for right (OD) and left (OS) eyes using ImageJ (Rasband, 1997). Each grid defined fourteen regions of interest (ROIs), representing inner (1), mid (2) and outer (3) portions of the superior (S), nasal (N), inferior (I) and temporal (T) central retina as well as the fovea and optic nerve head (ONH; see Supplementary Fig. 1). The relative position of the ONH with respect to the fovea was determined from baseline (pre-DLAAA injection) images for each eye and the ROI grid overlay then employed for all subsequent time points for that eye. Fluorescein signal intensity was evaluated within each ROI at each time point before normalization of these measurements according to relative differences in fluorescein intensity within the optic nerve head (where no DLAAA-induced leakage was observed) from week 10, immediately prior to intervention with aflibercept or saline. A mixed-effects analysis with repeated measures, followed by multiple comparisons test was performed in response to significant overall effects of treatment or time to evaluate differences in total leakage scores and fluorescein intensity. P values of 0.05 and below were considered statistically significant. All statistical analyses were performed using GraphPad Prism version 8.1.0 for Mac OS, GraphPad Software (San Diego, California USA, www.graphpad.com).

2.8. Optical coherence tomography

OCT was performed using a Spectralis OCT Plus system (Heidelberg Engineering, Vista, CA) with eye tracking and image capture and analysis software (HEYEX, Heidelberg Engineering, Vista, CA). An overall volume scan of the entire macula at a dense scan interval was performed at baseline, biweekly after DLAAA administration and weekly after intervention until study terminus. Dense retinal volume scans consisted of 48 parallel scans of 30° in the horizontal plane positioned 50 μm apart with image averaging over 50 ART frames with scan grid centered on the fovea. OCT image scans in the horizontal plane capturing the optic nerve head region and foveal region were exported as representative images to assess and demonstrate morphological changes.

2.9. Histopathological analysis

Two control and two DLAAA animals were euthanized and their eyes enucleated for histopathology. After removing the excess orbital tissue, eyes were placed in Davidson's Fixative for 24 hour followed by 10% neutral buffered formalin. One fixed eye from each animal was processed, embedded in paraffin, sectioned and stained by HSRL (Mount Jackson, VA) for histopathology, immunofluorescence (IF) and immunohistochemistry (IHC). Histopathology was performed on sections using standard Hemotoxylin and Eosin staining. IF was performed on additional sections of eyes using anti-glial fibrillary acidic protein (GFAP) primary antibody (Cell Signaling - 3670s, 1:500, 1 hour at room temperature), followed by incubation in AlexaFluor 488 secondary antibody (Invitrogen – A-11001, 1:1000, 30 minutes at room temperature). IHC was also performed using the following primary antibodies: anti-von Willebrand factor (vWF) (Thermo Scientific - MA514029, 1:200, 1 h at RT), anti-CD68 (Abcam – ab201340, 1:200, 1 h at RT), anti-CD105/endoglin (Abcam – ab219362, 1:1700, 1 h at

RT), anti-VEGF (Novus – NB100-664, 1:1000 at RT). This was followed by incubation in either Mouse on Farma HRP (Biocare Medical, BRR4002) or Rabbit on Farma HRP (Biocare Medical, BRR4009) and visualization using Betazoid DAB (Biocare Medical, BDB2004).

2.10. Clearing histology with multiphoton microscopy

Eyes were fixed in 4% paraformaldehyde for 4 hours and retinal whole mounts prepared by cutting radially at 4 quadrants for flattening. Retinal whole mounts were stained with DAPI and Eosin using proprietary methods developed by Applikate Technologies (Washington, DC), which involved a 2-hour stepwise dehydration in 75% ethanol and 100% ethanol, followed by 30-minutes clearing in benzyl alcohol/benzyl benzoate. Samples were imaged on a custom ultra-high speed, high resolution multiphoton microscope with an 80 MHz repetition rate pulsed laser and a long working distance index-matched objective (Olson et al., 2018). Data were collected at a pixel size of 250 nm for focal high-resolution 3D reconstructions or 1 μm for full resolution scanning. Whole retinal imaging took 5–8 hours. Retinal whole mounts were imaged at a depth of up to 600–1000 μm to account for sample irregularities. Axial step size varied from 1 μm for high resolution scans up to 10 μm for full reconstructions. Automated image processing routines were developed in Python including normalization, stitching, and pyramidal structuring for multi-zoom, multi-level visualization in StackStreamer software (www.stackstreamer.com). The processed images were further analyzed using ImageJ software.

3. Results

DLAAA administration disrupted retinal structural integrity and induced fluid accumulation, vessel tortuosity and pathologic vascular leakage and remodeling. FA imaging revealed hyperfluorescent leakage predominantly in the macular and perimacular regions starting at week two, with a small number of eyes displaying leakage stretching to the vascular arcades and periphery. The leakage progressed rapidly in the first 4 weeks, became stable within 8–10 weeks and persisted through week 18 and beyond (Fig. 1A). Additionally, enlargement of the foveal avascular zone with obliteration of the perifoveal capillary network was observed in some eyes. Evaluation of early phase FA (20–30 s) at weeks 4, 6 and 9 revealed evidence of neovascular vessels within the macular region (Fig. 1B). In addition, capillaries and microvasculature of the perifoveal region frequently exhibited abnormalities after DLAAA administration, with dilation and leakage, a hallmark of MacTel, widely evident during early phase FA imaging (Yannuzzi et al., 2006). Vessel pathology similar to MacTel was additionally evident by color fundus photography (Fig. 2). Fundoscopy and color fundus images revealed vascular occlusion in the macular region consistent with the angiographic data and clinical correlates. Additionally, areas of retinal whitening and particularly nerve fiber layer edema were observed consistent with hypoperfusion.

OCT revealed morphological changes associated with vascular leakage. At week 2 after DLAAA treatment, subfoveal disorganization and hyperreflectivity were evident. Extensive nerve fiber layer and inner retinal edema were observed, became prominent at week 4 and persisted through week 10; nerve fiber layer and inner retina edema were associated with pronounced hyperreflectivity with underlying shadowing, which completely obscured the underlying retina. These early pathological changes progressed to degenerative cystic changes and inner retinal atrophy at weeks 16 and 18. Retinal thickening was pronounced in the macular region from weeks 2–8, whereas retinal thinning occurred within the perimacular region throughout. Additionally, the lamellar structure of the retina was disorganized (Fig. 3). Posterior vitreous detachments and/or epiretinal membranes were evident in a few DLAAA-treated eyes one week after treatment and in some instances this response persisted up to 10 weeks (data not shown). These changes in the retinal architecture were observed prior to stabilization of chronic vascular leakage around 8–10 weeks after DLAAA injection and likely represent direct toxic and triggered inflammatory events induced by the glial toxin.

Histopathological and IHC evaluation of DLAAA retinal tissue revealed retinal degeneration. High-resolution multiphoton imaging of retinal whole mounts from healthy control and DLAAA-treated eyes revealed cellular injury and damage, including displaced nerve fiber layer and plexiform layers, distorted inner and outer nuclear layers with changes in distribution of nuclei within each layer compared to control retina. Additionally, signs of hemorrhage and disruption of vascular integrity were evident in the DLAAA retina by presence of red blood cells at both the inner retina surface and within the outer nuclear layer of the retina (Fig. 4).

DLAAA treatment induced retinal degeneration and pathological vascular remodeling. H&E evaluation of retinal sections from DLAAA-treated eyes 12 weeks after treatment revealed areas with proliferation and intraretinal neovascularization within a disorganized neuroretina. Retinal degeneration was more severe in the central retina (~3 mm from the optic nerve head), characterized by marked thinning of all layers and decreased cellularity of the inner and outer nuclear layers, photoreceptor layer and ganglion cell layer (Fig. 5A and 5C). In the peripheral retina, marked thinning and decreased cellularity of all layers were also observed (Fig. 5B and 5D). A similar degree of retinal degeneration was also evident at week 16 in DLAAA-treated eyes (Fig. 5E, 5F). Elevation of the inner limiting membrane and clefting were observed at the vitreoretinal surface and accompanied by microvasculature proliferation (Fig. 5F). Neovascular response was evident by H&E and further confirmed in DLAAA treated retinas by IHC staining. Within the inner retina expression patterns of vWF, revealing immature vasculature, coincided with CD105/endoglin staining of endothelial cells involved in neovascularization (Fig. 6A–D). IHC staining of VEGF in the control retina (Fig. 6E) revealed expression in the inner retinal layer cells and a degree of expression in the ganglion cell layer cells. DLAAA treated retinas exhibited similar levels of VEGF expression to controls, however, a pronounced signal was observed in the proliferative areas of the inner retina (Fig. 6G), which co-distributed with vWF, CD105/endoglin and CD68, indicative of macrophages/microglia infiltration (Fig. 6F and 6H). Together, these IHC stains confirmed pathological vascular remodeling in the DLAAA treated retina. GFAP staining revealed evidence of reactive gliosis throughout the peripheral retina (Fig. 7D) and near absence of GFAP-positive glial cells in the central retina (Fig. 7B, 7C). These changes were consistent with the observed central retinal degeneration and specific toxicity of DLAAA towards glial cell types. While GFAP staining was observed within the optic nerve in both control and DLAAA retinas, GFAP staining appeared to be more prominent in the optic nerve head region contiguous with the retina in the DLAAA-treated vs. control retina (Fig. 7A).

DLAAA administration at week 0 resulted in development of chronic vascular leakage that stabilized by weeks 8–10. The role of VEGF in vascular leakage induced by DLAAA was evaluated by assessing treatment response to IVT dosing with a clinically approved anti-VEGF therapy, aflibercept (Schmidt-Erfurth et al., 2014). The IVT dosing of saline and aflibercept were conducted ten weeks after DLAAA injection (defined here as “pre-dose”). Saline-treated eyes demonstrated no change in leakage from pre-dose until the study terminus at week 8 post-IVT dosing (week 18). IVT administration of aflibercept (35 μL of 40 mg/mL solution) resulted in marked reduction of leakage within 2 weeks, with maximum inhibition evident 2–4 weeks after dosing. Leakage recurred 6 weeks after dosing and reached a level similar to or slightly less than the pre-treatment levels 8 weeks following aflibercept administration (Fig. 8A). Analysis of graded clinical scoring using the established 10-point scale (Table 1) revealed that aflibercept significantly reduced leakage scores from pre-dose to week 4 (*$P = 0.0016$). No significant changes in clinical scores were observed following saline administration. A significant difference was observed between saline and aflibercept groups as early as week 2 post-treatment

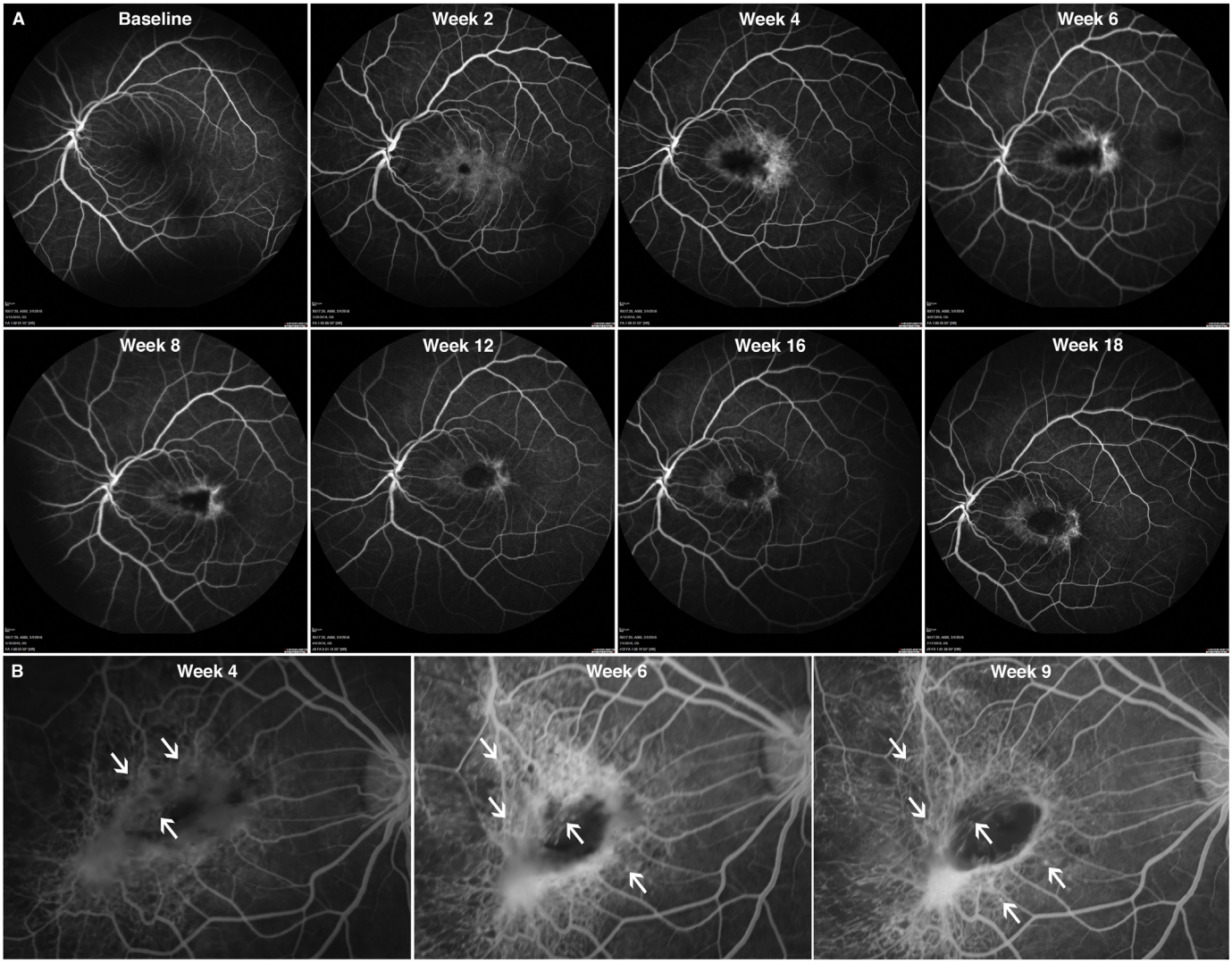

Fig. 1. Vascular leakage is sustained following intravitreal administration of DLAAA in monkeys. (**A**) Representative 1-minute fluorescein angiograms (FAs) were taken from baseline to week 18. Weekly FA exams revealed hyperfluorescent leakage in the macular and perimacular regions starting 2 weeks post-DLAAA administration. Vascular leakage progressed rapidly in the first 4 weeks, became stable by weeks 8–10, and then persisted through week 18 and beyond (see Fig. 9). (**B**) Representative early phase FA (20–30 seconds) images taken at weeks 4, 6 and 9 show evidence of neovascularization (see arrows) in the macular region including in the fovea.

($^{\#}$P = 0.0244) (Fig. 8B). Analysis of fluorescein signal intensity as a measure of vascular leakage from 1-minute FA images using the purpose-built multi-ROI grid in ImageJ revealed significant increases in fluorescein signal in response to DLAAA administration and significant subsequent reduction in this signal following IVT dosing with aflibercept. Saline administration did not significantly attenuate fluorescein leakage induced by DLAAA treatment (Fig. 8C and D).

In the absence of continuous intervention, DLAAA-induced vascular leakage persisted to the 98-week timepoint evaluated. The magnitude of vascular leakage was slightly diminished over extended study durations (90+ weeks) compared with observations in the same eyes 10–18 weeks after DLAAA treatment (Fig. 9A, D). The continued role of VEGF in persistent DLAAA-induced retinal vascular leakage was assessed by performing repeat IVT injection of aflibercept at 8 and 90 weeks post-DLAAA treatment in the same cohort of animals. Aflibercept attenuated DLAAA-induced leakage inhibition at both time points with maximal effect observed 4 weeks after treatment (Fig. 9B, E).

4. Discussion

DLAAA, a metabolite in the synthesis of lysine, does not exist in high concentrations within the retina; it may represent a biomarker of oxidative stress, as in the setting of hyperglycemia (Wijekoon et al., 2004; Yuan et al., 2011). DLAAA was first described as a glial toxin when evaluated for cytotoxicity in fetal mouse brain cells, as one of multiple acidic and sulfur containing amino acids screened (Olney et al., 1971). Ocular pathological manifestations of DLAAA administration are consistent with the known *in vitro* cytotoxic effects on Müller glial cells (Ishikawa and Mine, 1982). DLAAA damage to Müller cells have been demonstrated within 5 hours of intravitreal delivery in rodents. The damage has been characterized with light (Olney et al., 1971) and electron microscopy (Pedersen and Karlsen, 1979), as cytoplasmic vacuolization, decreased electron density and cell necrosis confined to Müller cells, while the retinal pigment epithelium, photoreceptors and retinal neurons remain relatively unchanged. To the extent early pathology defines the proximate susceptible cell type, these observations would implicate Müller injury as the precipitating event of DLAAA-induced retinal pathology. Functionally, this is corroborated by b-wave ERG signal loss (Newman and Odette, 1984; Welinder et al., 1982).

As such, retinal pathology induced by supra-physiological levels of intravitreal and retinal DLAAA is not inherently a direct model of the pathophysiology of neovascular AMD, diabetic macular edema, PDR,

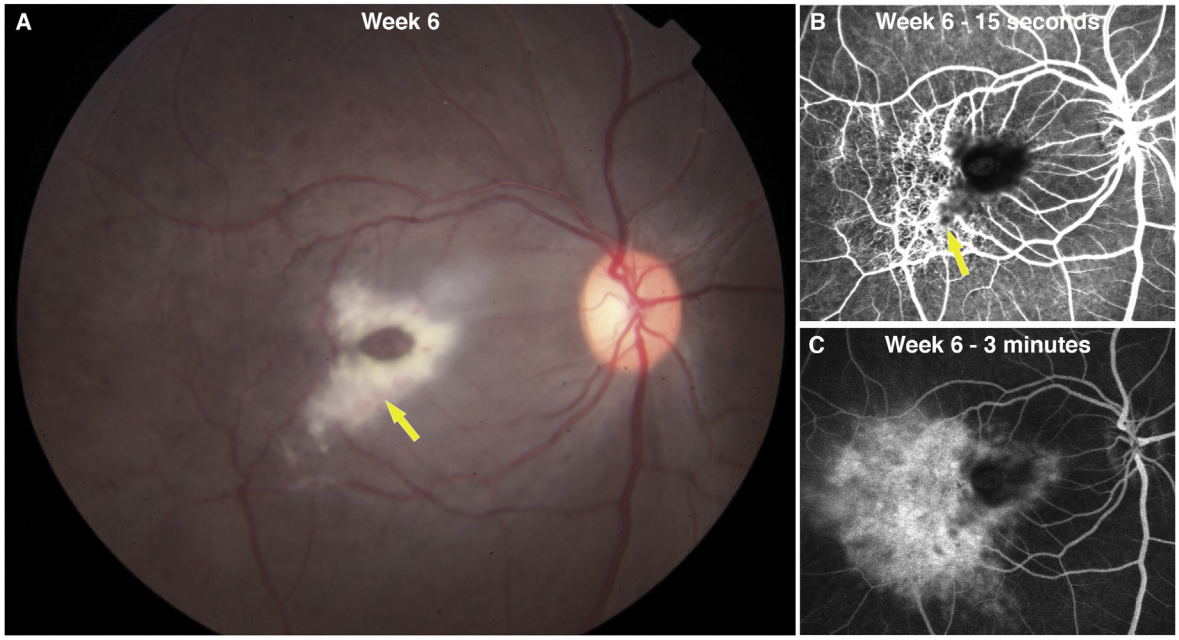

Fig. 2. Macular telangiectasias are feature of DLAAA pathology. (**A**) Representative color fundus photograph taken at week 6 post-DLAAA administration shows dilated and leaky macular telangiectatic vessels near the fovea (see yellow arrow) and vascular occlusion in the macular region. The corresponding 15 s (**B**) and 3-minute (**C**) FA series images also highlight the telangiectatic vessels (see yellow arrow). (For interpretation of the references to color in this figure legend, the reader is referred to the Web version of this article.)

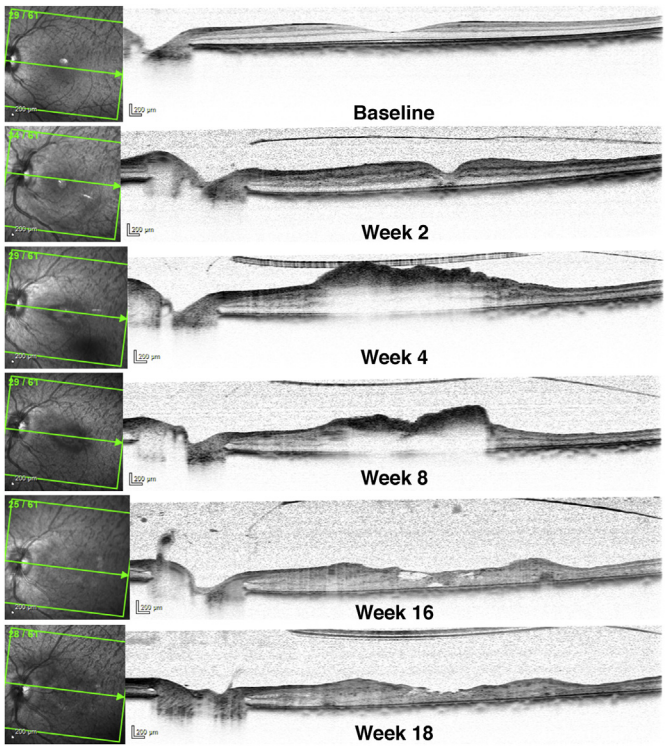

Fig. 3. OCT reveals morphological changes in the DLAAA retina. OCT exams revealed morphological changes associated with vascular leakage. Subfoveal disorganization and hyperreflectivity were evident at week 2. Extensive inner retinal edema became prominent starting at week 4 and sustained through week 10. Hyperreflectivity with underlying shadowing and hyporeflectivity at weeks 4 and 8 were also observed, followed by degenerative cystic changes and inner retinal atrophy at weeks 16 and 18. As a result, retinal thickening was pronounced in the macular region from weeks 4–8, whereas areas within the perimacular region showed retinal thinning throughout.

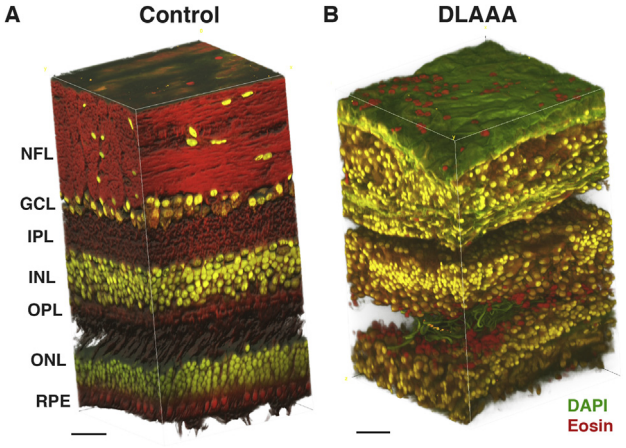

Fig. 4. DLAAA disrupts retinal structural integrity and promotes leakage. Three dimensional reconstructions of high-resolution multiphoton images acquired from full tissue depth tissue samples from control eyes (**A**) and eyes with DLAAA-induced retinal degeneration (**B**), revealing numerous fibrotic tangles (in green; likely from collagen detected through second-harmonic generation) at the displaced nerve fiber layer and in the outer nuclear layer, red blood cells in hemorrhagic areas, marked changes in distribution of nuclei and distortion of retinal layers. Scale bar – 20 μm. Abbreviations: NFL-nerve fiber layer, GCL-ganglion cell layer, IPL-inner plexiform layer, INL-inner nuclear layer, OPL-outer plexiform layer, ONL-outer nuclear layer, RPE-retinal pigment epithelium. (For interpretation of the references to color in this figure legend, the reader is referred to the Web version of this article.)

branched retinal vein occlusion, or other common RNVs or retinal ischemic conditions. The DLAAA-induced chronic vascular leak, however, does share elements of these conditions. The presence of retinal vessels with persisting pathologic endothelial leakage and detectable fluid exudation by FA are characteristics of neovascular AMD, DME and PDR. The vessel pathology observed in color fundus images suggests macular retinal vascular occlusion consistent with angiographic and OCT findings in retinal ischemic conditions. Evaluation of serial FA

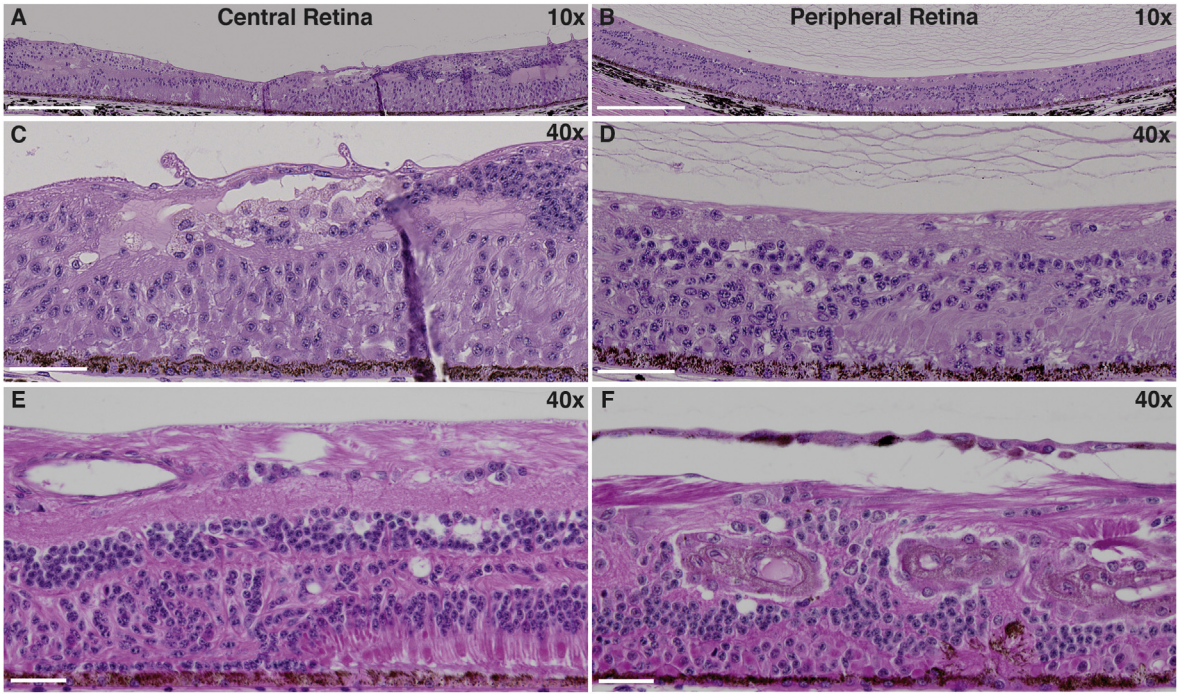

Fig. 5. Histology reveals retinal degeneration following intravitreal administration of DLAAA. Representative light photomicrographs of central and peripheral regions of hematoxylin and eosin stained paraffin sections of retina from week 12 (**A-D**) and week 16 (**E-F**) after DLAAA treatment. Marked retinal degeneration was observed throughout the retina, most prominent in the central retina with decreasing severity peripherally. (**A,C**) In the central retina (~3 mm from optic nerve head [ONH]), there was multifocal loss of the plexiform layers, marked thinning, disruption and disorganization of the nuclear layers with loss of distinction between the layers, marked loss of photoreceptors, and increased cellularity of the ganglion cell layer with few identifiable ganglion cells present. Areas with proliferation and intraretinal neovascularization were observed within a disorganized neuroretina. (**B,D**) In the peripheral retina (~7 mm from ONH), retinal degeneration consisted of marked thinning of all layers, decreased cellularity of the inner and outer nuclear layers, the photoreceptor layer and the ganglion cell layer. (**E-F**) Retinal degeneration at week 16 was comparable to week 12. Closer to the optic nerve (**E**), abrupt alterations in outer nuclear layer and obliteration of the inner/outer segments of rods and cones was evident due to proliferation of cells (gliosis) in the outer nuclear layer. (**F**) Both elevation of inner limiting membrane and clefting at the level of the ganglion cell layer were observed with superficial microvasculature proliferations within the limiting plate and perivascular melanin pigmentation. Scale bar – 250 μm (**A-B**) and 50 μm (**C–F**).

images suggests an occlusive component to the pathology confined to the inner to deep retinal capillary plexus. OCT findings demonstrated inner retinal edema, which is also consistent with ischemia and vascular occlusion. Moreover, responsiveness to anti-VEGF intervention and existence of neovessels support the additional involvement of a leaking capillary endothelium. DLAAA-induced pathology differs from neovascular AMD in that the neovascular vessels originate from the vasculature of the inner retina, and not the choroidal origin that is pathognomonic for neovascular AMD. While there is significant inner retinal edema in the macula in the early, immature DLAAA phenotype, the pathology differs from diabetic macular edema in that there is no significant retinal edema in its mature state, in part reflecting the degree of degeneration and thinning of all retinal layers that accompanies the DLAAA-induced lesion. Retinal distribution and angiographic characteristics of DLAAA lesions in the NHP share a number of characteristics with MacTel, including ectatic perifoveal capillaries, intraretinal neovascularization, right angle vascular telangiectasia, leakage and macular atrophy with photoreceptor loss, disruption of the outer limiting membrane, and retinal cavitation in inner retinal layers (Yannuzzi et al., 2006), although responsiveness to anti-VEGF is limited to proliferative forms with active neovascularization (Charbel Issa et al., 2016).

VEGF has been implicated in many retinal neovascular diseases, and is a mediator of DLAAA vascular permeability, as demonstrated by responsiveness of the leakage to anti-VEGF intervention in NHP, rabbit (Cao et al., 2018; Li et al., 2018; Rodrigues et al., 2018) and rat (Shen et al., 2010) models. In the latter model vitreous VEGF levels have been directly measured and correlated to pathology. Previous rabbit studies demonstrated a response to aflibercept with recurrence of leakage 8 weeks following 0.5 mg/eye of aflibercept (Cao et al., 2018), and 10 weeks following 1.2 mg/eye of aflibercept (Li et al., 2018), suggesting a dose response effect to the achieved aflibercept vitreous concentration of 0.33 mg/mL vs. 0.8 mg/mL, assuming a rabbit vitreous volume of 1.5 mL (Weir and Collins, 2013). African green monkey vitreous volume of 2.4–2.9 mL is nearly double [(Glogowski et al., 2012) and unpublished data] that of rabbits and the achieved concentration in this study was ~0.52 mg/mL, intermediate to explored rabbit concentrations. It is plausible and likely that the duration of action of aflibercept is also species dependent, reflecting differences in retinal anatomy and physiology. The observed recurrence of vascular leakage after drug washout in primates at 4–8 weeks following administration of human equivalent doses of aflibercept is more aligned with the clinical experience in active eAMD.

Prior studies employing subretinal delivery of DLAAA in NHPs did not identify significant retinal neovascularization (Shen et al., 2011). While subretinal delivery contributed to significant cone photoreceptor loss, it did not result in marked Müller cell loss at the doses evaluated (Shen et al., 2011). Subretinal DLAAA did result in marked neovascularization in the rat, which was also accompanied by significant Müller cell loss and elevations in VEGF (Shen et al., 2010). While these observations suggest possible species differences to susceptibility to DLAAA by different routes of administration, the correlation of Müller cell loss to neovascularization further implicates Müller cells in the chronic neovascular leakage phenotype achieved by DLAAA.

The plateau of persisting leakage is an important feature of the model. A decrease in leakage size and fluorescence intensity following IVT aflibercept treatment is observed, with maximal decrease four weeks post-treatment. The recurrence of leakage begins between weeks

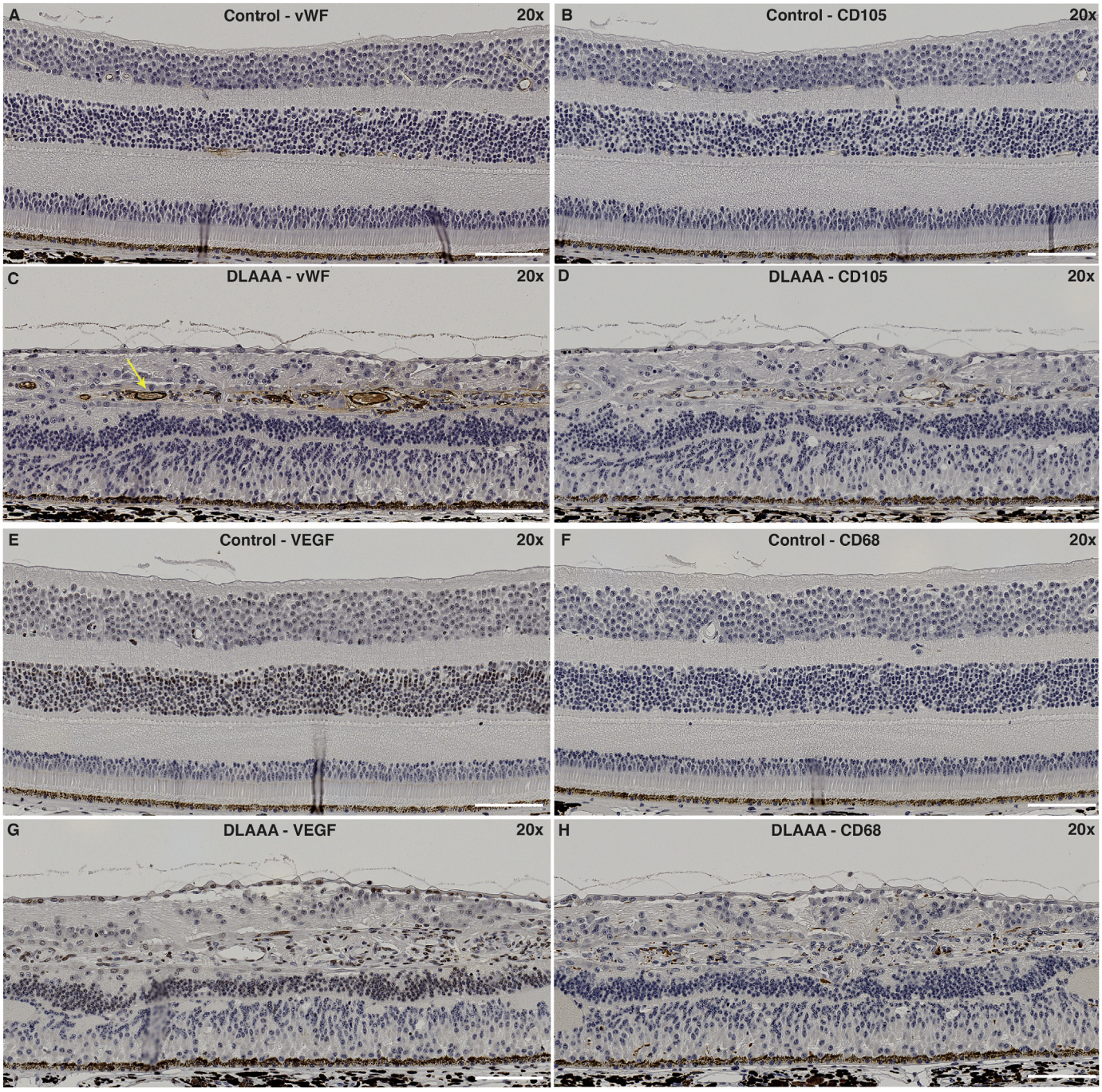

Fig. 6. Immunohistochemistry reveals pathological vascular remodeling. Chromogenic staining of von Willebrand Factor (vWF), a marker of endothelial cell activation, on paraffin sections of retina from control eye (**A**) demonstrated normal vascular structure throughout. DLAAA-treated eye (**C**) collected at week 12 revealed DLAAA-induced endothelial cell damage and proliferation predominantly within the inner retina. CD105/endoglin staining of DLAAA retina **(D)** revealed areas with neovascularization in the inner retina that coincided with vWF staining. VEGF reactivity in the control retina **(E)** was largely localized to inner retinal layer cells, however, VEGF reactivity in the DLAAA retina **(G)** was pronounced, especially in areas of proliferation and neovascularization. DLAAA retina **(H)** showed pronounced expression of CD68 positive infiltrating macrophages/microglia compared to control retina **(F)**. Representative images from the central retina ~3 mm from the ONH are presented; scale bar – 100 μm.

4–6 and reaches a level similar to or slightly less than the pre-treatment levels 8 weeks after aflibercept. The degree of subsidence of leakage in response to aflibercept treatment appears dependent on leakage area size and severity prior to treatment. The degree of response is additionally depended on the interval between the DLAAA induction and the aflibercept intervention, with early anti-VEGF intervention, that occurs within a period of ongoing remodeling, behaving differently than intervention at later more stable timepoints. Expanded longitudinal observation in larger treatment groups will be needed to fully characterize the correlation between leakage area size and severity and the achieved maximal percent and duration of inhibition.

Müller cells are centrally involved in retinal glutamate homeostasis (Voaden, 1976) and are critical to neurotransmitter recycling, including glutamate and glycine, and facilitate catabolism of other toxic metabolites such as ammonia in the highly metabolic environment of the retina (Bringmann et al., 2006). Müller cells sustain a higher capacity

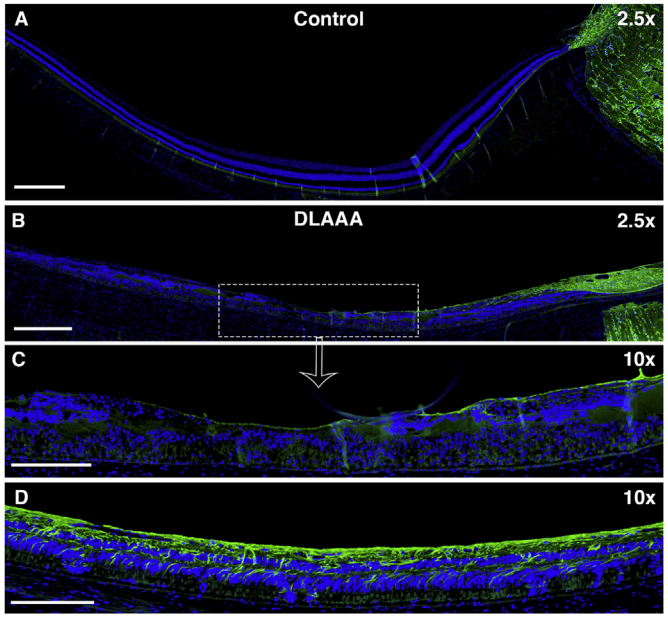

Fig. 7. GFAP immunostaining demonstrates Müller cell damage in the DLAAA retina. Representative immunofluorescence images of retina from control (**A**) and DLAAA-treated eyes (week 12) (**B–C**) showed reduced expression of glial fibrillary acidic protein (GFAP) in the central retina due to DLAAA-induced degeneration (representative area illustrated in panel B is shown in panel C) and (**D**) elevated expression in the peripheral retina with evidence of astrogliosis, compared to lower expression (**A**) in the healthy control retina. (**B**) The retina and optic nerve head transition area illustrated pronounced GFAP signal in the DLAAA-treated vs. control retina. Scale bar – 500 μm (**A-B**) and 200 μm (**C-D**).

for these functions than surrounding neurons, to which they supply critical support as the principal glial cells of the retina. Müller cells interface directly with retinal blood vessels, contributing to the barrier properties of the vessels, as well as the cytokine signaling that mediate neurovascular coupling (Coughlin et al., 2017). The loss of these Müller cell functions likely contributes to the direct association between Müller cell destruction and chronic vascular leakage.

Populations of Müller cells in primates exhibit regional and morphologic differences. The foot processes of macular Müller cells are located in Henle's fibers close to reservoirs of photooxidative stress-reducing xanthophylls, lutein and zeaxanthin (Gass, 1999). Müller cells in the macula may be further distinguished from those of the peripheral retina by significantly different gene transcription of mediators of serine synthesis, glycolytic function and mitochondrial metabolism (Zhang et al., 2019). Phosphoglycerate dehydrogenase (PHGDH), the rate-limiting enzyme in serine synthesis and redox homeostasis is markedly upregulated in macular Müller cells, and both systemic and intravitreal L-serine have been demonstrated to rescue retinal function (Staubli et al., 2016). Notably, genome-wide analysis of patients with idiopathic juxtafoveal retinal telangiectasia type 2 (MacTel type 2) has identified a causative disease loci to be associated with the glycine/serine metabolic pathway (Scerri et al., 2017). This would suggest that macular Müller cells tuned to positively regulate oxidative stress by heightened serine production, endanger the macula when selectively impaired, either by mutations impacting serine biosynthesis (MacTel), or hyperphysiolgical exposure to metabotoxins such as DLAAA.

These regional differences in Müller cell physiology may explain the unique foveal and/or juxtafoveal pattern of DLAAA-induced pathology in foveated, holangiotic NHPs. DLAAA-induced leakage in the rabbit arises from retinal neovascularization in the avascular zone, contributing to linear regions of leakage overlapping the visual streak (Cao et al., 2018), where proximity to injection site appears be a determinant of lesion location. The retina of the primate, rabbit and rodent differ in properties of the ILM and OLM, related to relative Müller glia

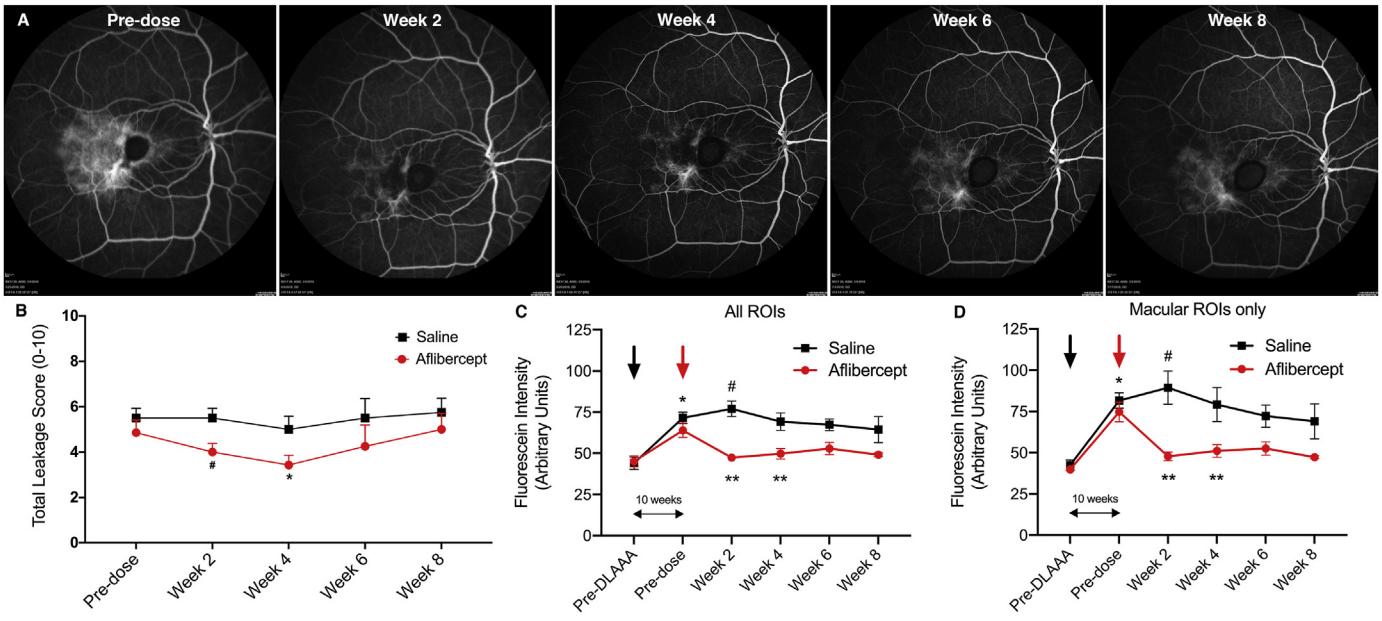

Fig. 8. DLAAA-induced retinal vascular leakage is VEGF-dependent. FA imaging at week 10 post-DLAAA administration (labeled as "pre-dose") and biweekly from weeks 2–8 following aflibercept administration (35 μL of 40 mg/mL solution). Image evaluations revealed marked attenuation of DLAAA-induced retinal vascular leakage beginning at week 2 and through week 4, with subsequent return of leakage from weeks 4–8 after aflibercept dosing (**A**). Fluorescein leakage was assessed by graded scoring (**B**) using a 10-point scale (see Table 1) and by computer-based analysis of leakage intensity using ImageJ (**C-D**). Leakage was most significantly attenuated from pre-dose measures at 2–4 weeks post-dosing. Values represent mean total leakage score from n = 4–7 eyes/group, vertical bars represent the SEM. (**B**) *P = 0.0016 vs. corresponding pre-dose measurement, #P = 0.0244 vs. week 2 saline treatment. (**C-D**) Black arrows indicate time of DLAAA injection. Red arrows indicate intervention with Eylea or saline. *P < 0.05 vs. pre-DLAAA; **P < 0.05 vs. corresponding pre-dose measurement; #P < 0.05 vs. corresponding time point for saline-treated eyes. (For interpretation of the references to color in this figure legend, the reader is referred to the Web version of this article.)

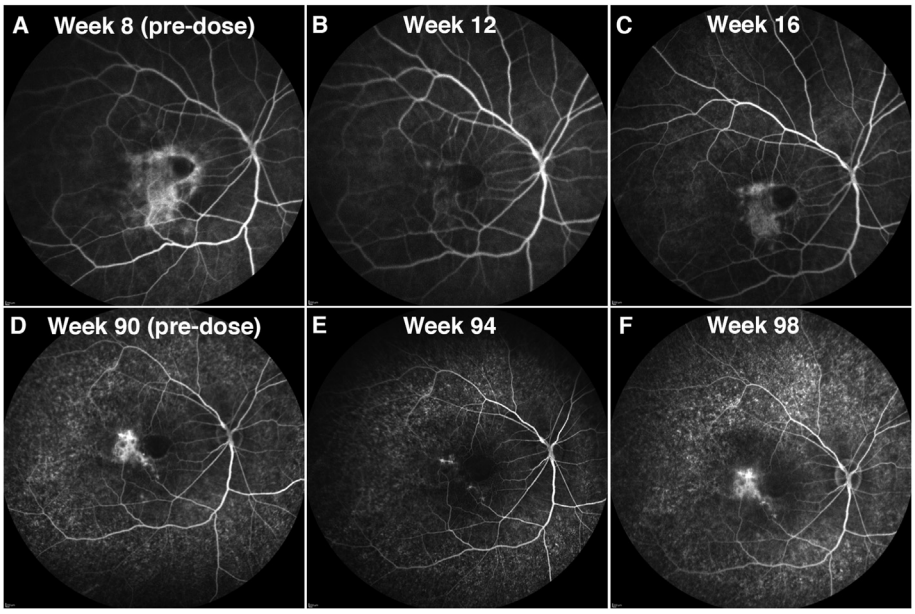

Fig. 9. DLAAA-induces long term VEGF-dependent retinal vascular leakage. FA imaging was performed at 8 (**A**) and 90 (**D**) weeks (labeled as "pre-dose") after DLAAA-administration in the same eye, revealing sustained vascular leakage within the macula. Both the first and second intravitreal dose of aflibercept (35 μl of 40 mg/mL solution) significantly inhibited retinal vascular leakage, peaking around 4 weeks post-dosing (labeled as week 12 (**B**) and week 94 (**E**)), with gradual recurrence of leakage to a level similar to or slightly less than the pre-dose condition 8 weeks after aflibercept dosing (labeled as week 16 (**C**) and week 98 (**F**)). Confluent, small window defects were observed in the angiogram during long term follow-ups, reflecting RPE defects, choroidal fluorescence and potential fibrosis.

configurations, and possibly contributing to differing DLAAA-induced retinal morphological changes. The greater degree of observed inner retinal edema and vascular leakage and remodeling in the NHP are prominent features that expand translational relevance of retinal vascular diseases such as diabetic retinopathy and retinal vein occlusion.

DLAAA-induced leakage evaluated through the applied clinical grading scale and a multi-ROI automated analysis tool, both of which quantified leakage size and severity based on fluorescence intensity, revealed a significant reduction in leakage size/severity and fluorescein signal following IVT dosing with aflibercept. Limiting the automated analysis evaluation to those ROIs most commonly demonstrating leakage, increased the dynamic range of the quantification. However, macular holes, and variable FA image positioning and quality, secondary to corneal integrity and the achieved mydriasis, impacted some comparisons, highlighting the importance of reducing the technical variability of image acquisition for automated analyses. Graded scoring using the developed 10-point scale lacks the regional specificity and dynamic range of computer-based analyses, but comprehensively ranks size and severity of leakage, allowing meaningful interpretation of the effect of intervention that is less sensitive to image quality. Applying both complementing quantification strategies improves the robustness of the overall evaluation.

Despite the success of existing anti-VEGF therapies to combat retinal neovascular disease there is significant need for improved therapeutics for subjects refractory to standard of care, and for a longer duration of action. This clinical need, in turn, demands improved means by which to select and refine candidates in the preclinical setting. Applying DLAAA to elicit a chronic retinal neovascular leakage phenotype in the NHP provides distinct advantages over other preclinical neovascular models of retinal vascular leakage. Models such as laser-induced CNV or branched retinal vein occlusion are more transient and typically do not guide pharmacodynamic assessment of duration of effect often critical to clinical success and important to define in early stages of therapeutic development. Employing the DLAAA model in primates provides advantages over other species, mirroring aspects of macular pathology common to neovascular AMD, PDR and MacTel. Furthermore, expanding evaluation of antibody and gene therapy-based approaches demands test systems with the immunologic and genetic homology of Old World primates to chart safe and de-risk paths to clinic. Specific benefits of our described approach to the application of the DLAAA model in the NHP include consistent induction through a titrated dose and applied, clinically-relevant imaging modalities and methods. The customized clinical grading scale and multi-ROI automated analysis tool provide complementary quantification of documented vascular leakage.

Funding sources

Richard Torres acknowledges support from grant 3UL1TR001863 from the National Center for Advancing Translational Science (NCATS) and R43 EB21171-01 from the National Cancer Institute of the U.S. National Institutes of Health.

Appendix A. Supplementary data

Supplementary data to this article can be found online at https://doi.org/10.1016/j.exer.2020.108031.

References

Antonetti, D.A., Klein, R., Gardner, T.W., 2012. Diabetic retinopathy. N. Engl. J. Med. 366, 1227–1239.
Bringmann, A., Pannicke, T., Grosche, J., Francke, M., Wiedemann, P., Skatchkov, S.N., Osborne, N.N., Reichenbach, A., 2006. Muller cells in the healthy and diseased retina. Prog. Retin. Eye Res. 25, 397–424.
Cao, J., MacPherson, T.C., Iglesias, B.V., Liu, Y., Tirko, N., Yancopoulos, G.D., Wiegand, S.J., Romano, C., 2018. Aflibercept action in a rabbit model of chronic retinal neovascularization: reversible inhibition of pathologic leakage with dose-dependent duration. Invest. Ophthalmol. Vis. Sci. 59, 1033–1044.
Charbel Issa, P., Kupitz, E.H., Heeren, T.F.C., Holz, F.G., 2016. Retinal diseases amenable to pharmacotherapy. In: Nguyen, Q.D., Rodrigues, E.B., Farah, M.E., Mieler, W.F., Do, D.V. (Eds.), Retinal Pharmacotherapeutics. Karger, Basel, pp. 189–195.
Coughlin, B.A., Feenstra, D.J., Mohr, S., 2017. Muller cells and diabetic retinopathy. Vision Res 139, 93–100.
Gass, J.D., 1999. Muller cell cone, an overlooked part of the anatomy of the fovea centralis: hypotheses concerning its role in the pathogenesis of macular hole and foveomacualr retinoschisis. Arch. Ophthalmol. 117, 821–823.
Glogowski, S., Ward, K.W., Lawrence, M.S., Goody, R.J., Proksch, J.W., 2012. The use of the African green monkey as a preclinical model for ocular pharmacokinetic studies. J. Ocul. Pharmacol. Therapeut. 28, 290–298.
Grossniklaus, H.E., Kang, S.J., Berglin, L., 2010. Animal models of choroidal and retinal neovascularization. Prog. Retin. Eye Res. 29, 500–519.
Ishikawa, Y., Mine, S., 1982. [Structural changes in retinal glial cells following the intravitreal injection of DL-alpha-aminoadipic acid]. Nippon. Ganka Gakkai Zasshi 86, 810–820.
Kato, S., Ishita, S., Sugawara, K., Mawatari, K., 1993. Cystine/glutamate antiporter expression in retinal Muller glial cells: implications for DL-alpha-aminoadipate toxicity. Neuroscience 57, 473–482.
Kato, S., Sugawara, K., Matsukawa, T., Negishi, K., 1990. Gliotoxic effects of alpha-aminoadipic acid isomers on the carp retina: a long term observation. Neuroscience 36, 145–153.

Li, Y., Busoy, J.M., Zaman, B.A.A., Tan, Q.S.W., Tan, G.S.W., Barathi, V.A., Cheung, N., Wei, J.J., Hunziker, W., Hong, W., Wong, T.Y., Cheung, C.M.G., 2018. A novel model of persistent retinal neovascularization for the development of sustained anti-VEGF therapies. Exp. Eye Res. 174, 98–106.

Linser, P.J., Moscona, A.A., 1981. Induction of glutamine synthetase in embryonic neural retina: its suppression by the gliatoxic agent alpha-aminoadipic acid. Brain Res. 227, 103–119.

Liu, Y.C., Ng, A.H.C., Ng, X.W., Yan, P., Venkatraman, S.S., Mehta, J.S., Wong, T.T., 2017. Evaluation of a sustained-release prednisolone acetate biodegradable subconjunctival implant in a non-human primate model. Transl Vis Sci Technol 6, 9.

Mustari, M.J., 2017. Nonhuman primate studies to advance vision science and prevent blindness. ILAR J. 58, 216–225.

Newman, E.A., Odette, L.L., 1984. Model of electroretinogram b-wave generation: a test of the K+ hypothesis. J. Neurophysiol. 51, 164–182.

Olney, J.W., Ho, O.L., Rhee, V., 1971. Cytotoxic effects of acidic and sulphur containing amino acids on the infant mouse central nervous system. Exp. Brain Res. 14, 61–76.

Olson, E., Levene, M.J., Torres, R., 2018. High-quality Histology of Cleared Tissue Samples by Polygon-Based Multiphoton Microscopy, Microscopy Histopathology and Analytics. Optical Society of America.

Pedersen, O.O., Karlsen, R.L., 1979. Destruction of Muller cells in the adult rat by intravitreal injection of D,L-alpha-aminoadipic acid. An electron microscopic study. Exp. Eye Res. 28, 569–575.

Rasband, W.S., 1997-2018. ImageJ. U. S. National Institutes of Health, Bethesda, Maryland, USA. https://imagej.nih.gov/ij.

Rodrigues, G.A., Mason, M., Christie, L.A., Hansen, C., Hernandez, L.M., Burke, J., Luhrs, K.A., Hohman, T.C., 2018. Functional characterization of abicipar-pegol, an anti-VEGF DARPin therapeutic that potently inhibits angiogenesis and vascular permeability. Invest. Ophthalmol. Vis. Sci. 59, 5836–5846.

Scerri, T.S., Quaglieri, A., Cai, C., Zernant, J., Matsunami, N., Baird, L., Scheppke, L., Bonelli, R., Yannuzzi, L.A., Friedlander, M., MacTel Project, C., Egan, C.A., Fruttiger, M., Leppert, M., Allikmets, R., Bahlo, M., 2017. Genome-wide analyses identify common variants associated with macular telangiectasia type 2. Nat. Genet. 49, 559–567.

Schmidt-Erfurth, U., Kaiser, P.K., Korobelnik, J.F., Brown, D.M., Chong, V., Nguyen, Q.D., Ho, A.C., Ogura, Y., Simader, C., Jaffe, G.J., Slakter, J.S., Yancopoulos, G.D., Stahl, N., Vitti, R., Berliner, A.J., Soo, Y., Anderesi, M., Sowade, O., Zeitz, O., Norenberg, C., Sandbrink, R., Heier, J.S., 2014. Intravitreal aflibercept injection for neovascular age-related macular degeneration: ninety-six-week results of the VIEW studies. Ophthalmology 121, 193–201.

Shen, W., Li, S., Chung, S.H., Gillies, M.C., 2010. Retinal vascular changes after glial disruption in rats. J. Neurosci. Res. 88, 1485–1499.

Shen, W., Zhang, J., Chung, S.H., Hu, Y., Ma, Z., Gillies, M.C., 2011. Submacular DL-alpha-aminoadipic acid eradicates primate photoreceptors but does not affect luteal pigment or the retinal vasculature. Invest. Ophthalmol. Vis. Sci. 52, 119–127.

Staubli, U., Rangel-Diaz, N., Alcantara, M., Li, Y.X., Yang, J.Y., Zhang, K.M., Foster, A.C., 2016. Restoration of visual performance by d-serine in models of inner and outer retinal dysfunction assessed using sweep VEP measurements in the conscious rat and rabbit. Vision Res 127, 35–48.

Voaden, M.J., 1976. Gamma-aminobutyric Acid and glycine as Retinal Neurotransmitters. Pergamon, Oxford.

Weir, A., Collins, M., 2013. Assessing Ocular Toxicology in Laboratory Animals. Humana, New York.

Welinder, E., Textorius, O., Nilsson, S.E., 1982. Effects of intravitreally injected DL-alpha-aminoadipic acid on the c-wave of the D.C.-recorded electroretinogram in albino rabbits. Invest. Ophthalmol. Vis. Sci. 23, 240–245.

Wijekoon, E.P., Skinner, C., Brosnan, M.E., Brosnan, J.T., 2004. Amino acid metabolism in the Zucker diabetic fatty rat: effects of insulin resistance and of type 2 diabetes. Can. J. Physiol. Pharmacol. 82, 506–514.

Yannuzzi, L.A., Bardal, A.M., Freund, K.B., Chen, K.J., Eandi, C.M., Blodi, B., 2006. Idiopathic macular telangiectasia. Arch. Ophthalmol. 124, 450–460.

Yuan, W., Zhang, J., Li, S., Edwards, J.L., 2011. Amine metabolomics of hyperglycemic endothelial cells using capillary LC-MS with isobaric tagging. J. Proteome Res. 10, 5242–5250.

Zhang, T., Zhu, L., Madigan, M.C., Liu, W., Shen, W., Cherepanoff, S., Zhou, F., Zeng, S., Du, J., Gillies, M.C., 2019. Human macular Muller cells rely more on serine biosynthesis to combat oxidative stress than those from the periphery. Elife 8.